Molecular Crystals and Liquid Crystals Science and Technology. Section A. Molecular Crystals and Liquid Crystals

Publication details, including instructions for authors and subscription information:
http://www.tandfonline.com/loi/gmcl19

Microconfined Liquid Crystals: Surface Induced Deformations, Ordering and Fluctuations

S. [Zcirc]umer [a] , A. Borŝtnik [a] , G. Skaĉej [a] , P. Ziherl [a] & G. P. Crawford [b]

[a] Physics Department, University of Ljubljana, Jadranska 19, 1000, Ljubljana, Slovenia

[b] Division of Engineering, Brown University, Providence, RI, 02912, USA

Version of record first published: 04 Oct 2006

To cite this article: S. [Zcirc]umer, A. Borŝtnik, G. Skaĉej, P. Ziherl & G. P. Crawford (1997): Microconfined Liquid Crystals: Surface Induced Deformations, Ordering and Fluctuations, Molecular Crystals and Liquid Crystals Science and Technology. Section A. Molecular Crystals and Liquid Crystals, 304:1, 477-494

To link to this article: http://dx.doi.org/10.1080/10587259708046999

Mol. Cryst. Liq. Cryst., 1997, Vol. 304, pp. 477–494
Reprints available directly from the publisher
Photocopying permitted by license only

Microconfined liquid crystals: surface induced deformations, ordering and fluctuations

S. Žumer, A. Borštnik, G. Skačej, P. Ziherl
Physics Department, University of Ljubljana, Jadranska 19, 1000 Ljubljana, Slovenia

and G. P. Crawford
Division of Engineering, Brown University, Providence RI 02912, USA

Abstract

Some recent results of the studies of subsurface deformations, splay-bend elasticity and surface-induced order in confined liquid crystals are presented. The subsurface deformations are studied using molecular description of the ordering, and Landau-de Gennes approach is used to interpret a DNMR study of wetting transitions in microconfined 5CB and for the analysis of fluctuations and forces in partially ordered nematic systems.

PACS number(s): 61.30.Cz, 61.30.Gd, 64.70.Md, 68.45.Gd

1 Introduction

The phrase "microconfined liquid crystals" is a synonym for liquid crystalline systems confined or constrained on (sub)micron scale within cavities with nontrivial geometry. Among these, dispersions of low molecular weight liquid crystals and polymers with polymer concentration ranging from 2% up to 80% are particularly important. In 1986, Doane and coworkers introduced polymerization-induced phase separation to form droplets within a solid polymer binder [1]. The resulting composite material — polymer dispersed liquid crystals (PDLC's) — and, to some extent, also materials formed by encapsulation [2] are characterized by a controlled droplet size distribution necessary for electro-optical applications. In the zero-field state, the composite strongly scatters light, but it can be reversibly switched to a transparent mode by applying an electric field, which aligns the droplets such that their refractive index matches the index of the polymer, thereby reducing the scattering power of the material. This mechanism can be used for various electro-optical applications such as light shutters for optical signal processing, switchable windows, large flat-panel displays, high definition projection systems, etc. [3].

With the discovery of PDLC materials and with the growing number of their applications, microconfined liquid crystals became one of the most active fields of liquid crystal research. Supramicron liquid crystalline droplets are most easily studied by optical polarizing microscopy [4], whereas in case of submicron size droplets the deuterium nuclear magnetic resonance (DNMR) is more appropriate. Although this technique is integrative, it can be of great help in the identification of the nematic order in cavity sizes as small as 0.01 μm [5]. The need for a well characterized confining geometry stimulated studies on liquid crystal confined to submicrometer cylindrical cavities of polymeric or aluminum oxide microporous membranes [6]. The walls of these cavities can be easily treated by chemical agents, which determine the anchoring strength and the direction of the easy axis. On the other hand, random porous materials are also becoming very popular media for studies of the effects of random confinement on liquid crystals [7, 8, 9]. These systems are most frequently studied by NMR techniques, light scattering, calorimetry, and X-ray scattering.

The theoretical description of the behavior of the microconfined liquid crystals is essential for interpretation of experimental studies of these rather complex systems and for understanding of their applicability. The approaches based on statistical mechanics usually do not go beyond the mean field approximation even for simple intermolecular potentials. Monte Carlo and molecular dynamics analyses are still rather limited in giving more than a qualitative insight in confined systems [10, 11]. Thus, the range of suitable theoretical methods is reduced to phenomenological approaches, i.e., to Landau-de Gennes theory based on either scalar or tensorial order parameter and to Frank elastic theory, in which the liquid crystalline ordering is described by the director field.

In present review of our recent work some questions related to the surface effects in the microconfined systems are addressed. In Section 2 the occurrence of subsurface deformations is discussed using a simple molecular model. Ordering, fluctuations, and forces in the partially ordered paranematic phase are treated in Section 3.

2 Subsurface deformations: a molecular picture

The first descriptions of liquid crystals in curved geometries were based on Frank elastic energy of the director field $\mathbf{n}(\mathbf{r})$ without the divergence terms

$$f_F = \frac{1}{2}K_{11}[\nabla \cdot \mathbf{n}]^2 + \frac{1}{2}K_{22}[\mathbf{n} \cdot (\nabla \times \mathbf{n})]^2 + \frac{1}{2}K_{33}[\mathbf{n} \times (\nabla \times \mathbf{n})]^2 \qquad (1)$$

and with the assumption of the strong anchoring [12]. The three elastic constants correspond to three independent elastic modes: splay (K_{11}), twist (K_{22}), and bend (K_{33}). In studies of PDLC's, it became clear that usually anchoring cannot be taken as strong and that the saddle-splay (K_{24}) elasticity

$$f_{24} = -K_{24}\nabla \cdot [\mathbf{n}(\nabla \cdot \mathbf{n}) + \mathbf{n} \times (\nabla \times \mathbf{n})], \qquad (2)$$

is crucial for the understanding of liquid crystalline structures in spherical cavities [13, 14]. The relevance of the mixed splay-bend (K_{13}) elastic contribution to the free energy

$$f_{13} = K_{13}\nabla \cdot [\mathbf{n}(\nabla \cdot \mathbf{n})], \tag{3}$$

is less clear. Long ago it has been shown that nonzero K_{13} elastic constant leads to an unbounded subsurface deformation [15] if stabilizing higher order terms in free energy are not taken into account [16]. The possible existence of strong although finite subsurface deformation poses doubt about macroscopic description [17]. To throw additional light on this question, we decided to investigate a simple molecular model.

2.1 Lattice model

We consider anisotropic molecules described by molecular directors $\mathbf{n}$. The intermolecular pairwise interaction for two molecules characterized by directors $\mathbf{n} = \mathbf{n}(\mathbf{R})$ and $\mathbf{n}' = \mathbf{n}(\mathbf{R}')$ and separated by the vector $\mathbf{r} = \mathbf{R}' - \mathbf{R}$ is modeled by

$$g(\varepsilon, C; \mathbf{n}, \mathbf{n}', \mathbf{r}) = -\frac{C}{r^6}\left[\mathbf{n}\cdot\mathbf{n}' - 3\frac{\varepsilon}{r^2}(\mathbf{n}\cdot\mathbf{r})(\mathbf{n}'\cdot\mathbf{r})\right]^2, \tag{4}$$

where ε is a parameter of intermolecular interaction anisotropy, which can be varied between 0 and 1, and $C > 0$ is the interaction strength. $\varepsilon = 1$ corresponds to the induced dipole-induced dipole coupling, whereas $\varepsilon = 0$ describes the isotropic interaction of Maier-Saupe type.

The model interaction between a liquid crystal molecule and substrate is of the same form [Eq. (4)] but with $C \to C_S$, $\varepsilon = 0$ and $\mathbf{n}' \to \mathbf{\Pi}$ (easy axis of the surface). This expression resembles Rapini-Papoular-like anchoring characterized by the strength $C_S > 0$. For convenience we introduce the ratio $W_S = C_S/C$, which measures the relative strength of the nematic-substrate and nematic-nematic interactions.

Since we neglect the temperature effects, the equilibrium state will be characterized by the minimum of the total free energy (F). To make the calculations as simple as possible, we use a lattice model and assume that the molecules can rotate only in the planes parallel to the xz plane, which is perpendicular to the substrate. To avoid the existence of the easy axis in the bulk, we chose a hexagonal lattice in xz plane with layer spacing $p \to \rho_0$ (ρ_0 is a molecular dimension; $\sim$1 nm); see Fig. 1. We consider a slab of N molecular layers between two substrates. In the slab, the director is parametrized by the tilt angle φ between the director and the surface normal: $\mathbf{n} = (\sin\varphi, 0, \cos\varphi)$, where $\varphi = \varphi(z)$. In fact, the dependence $\varphi = \varphi(z)$ has to be discretized according to the distribution of molecules in the sample. The same tilt angle $\phi(k)$ is thus assigned to all molecules in the k^{th} molecular layer ($z = const.$). Both bounding substrates are taken to have M layers and to induce easy orientations ϕ_0 and ϕ_1, respectively. In this analysis, we are going to study only the cases with symmetric external anchoring, where $\phi_0 = \phi_1$.

The position of each molecule is determined by a set of three numbers $\{\alpha, \beta, \gamma\}$, which are related to the spatial Cartesian coordinates x, y, z as follows: $x = p[2\alpha + \delta(\gamma)]/\sqrt{3}$,

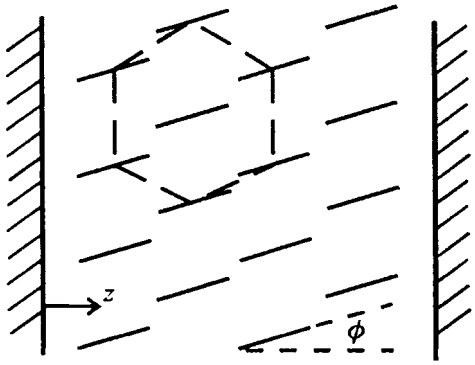

Figure 1: The hexagonal lattice between parallel plates and the definition of the tilt angle.

$y = p\beta$ and $z = p\gamma$. The function $\delta(\gamma)$ is equal to 1 if γ is even and 0 otherwise. In this way we can exploit the summation procedures already developed for the cubic lattice by Barbero et al. [18]. When performing the sum, we consider molecules with positions $\{0,0,m\}$ and $\{\alpha,\beta,\gamma\}$, their directors being $\mathbf{n}$ and $\mathbf{n}'$ tilted by $\phi(m)$ and $\phi(\gamma)$, respectively. The intermolecular vector is given by $\mathbf{r}(m;\alpha,\beta,\gamma) = p([2\alpha + \delta(\gamma) - \delta(m)]/\sqrt{3}, \beta, \gamma - m)$. The total interaction energy calculated per unit surface can thus be written as

$$F_i = \frac{1}{2p^2}\sum_{m=1}^{N}\sum_{\gamma=1}^{N}\sum_{\alpha=-\infty}^{\infty}\sum_{\beta=-\infty}^{\infty} g\left(\varepsilon, C; \mathbf{n}(m), \mathbf{n}(\gamma), \mathbf{r}(m;\alpha,\beta,\gamma)\right) \tag{5}$$

$$+\frac{1}{p^2}\sum_{m=-M+1}^{0}\sum_{\gamma=1}^{N}\sum_{\alpha=-\infty}^{\infty}\sum_{\beta=-\infty}^{\infty} g\left(0, C_s; \mathbf{n}(\gamma), \mathbf{\Pi}_0, \mathbf{r}(m;\alpha,\beta,\gamma)\right) \tag{6}$$

$$+\frac{1}{p^2}\sum_{m=N+1}^{N+M}\sum_{\gamma=1}^{N}\sum_{\alpha=-\infty}^{\infty}\sum_{\beta=-\infty}^{\infty} g\left(0, C_s; \mathbf{n}(\gamma), \mathbf{\Pi}_1, \mathbf{r}(m;\alpha,\beta,\gamma)\right), \tag{7}$$

where $\gamma = m, \alpha = 0, \beta = 0$ is excluded from the first sum.

In order to be able to cover also the external magnetic field effects, the corresponding energy F_m has to be taken into account. The magnetic energy per unit surface is obtained by summing over N of molecules with anisotropy of the molecular susceptibility χ_a and volume V_0 [19]:

$$F_m = -\frac{1}{2p^2} V_0 \mu_0 \chi_a \sum_{\gamma=1}^{N} \left[\mathbf{n}(\gamma)\cdot\mathbf{H}\right]^2. \tag{8}$$

The magnetic field strength H is for convenience furtheron expressed in terms of the dimensionless parameter $W_H = V_0 p^6 \mu_0 \chi_a H^2/2C$, which measures the strength of the magnetic field compared to the strength of nematic-nematic interactions.

The total energy of the sample $F = F_i + F_m$ is thus composed of bulk, surface and field contributions, which compete in causing deformations in the equilibrium state. To determine the equilibrium structure the total energy F must be minimized with respect

to all variables $\phi(k)$. This is accomplished by setting

$$\frac{\partial F}{\partial \phi(k)} = 0, \tag{9}$$

and $\partial^2 F/\partial\phi(k)^2 > 0$ for every $k \in [1, N]$ and then solving the system of non-linear equations (9). For an appropriate initial guess for the profile, this can be done, e.g., with the multidimensional Newton "tangential" method.

First we consider a nematic slab not influenced by any field or surface interaction. The solution for the molecular directors with the lowest energy is either planar ($\varepsilon = 1$) or homeotropic ($\varepsilon = 0.1$) undistorted alignment. If possible non-nematic "solid state solutions" with periodically modulated molecular director are excluded, one finds that any tilted director alignment has higher energy, which we interpret as *intrinsic anchoring*. It is due to incomplete intermolecular interactions close to the wall and has thus an intrinsic origin. In Fig. 2, the energy of the undistorted sample is plotted as a function of the tilt angle and shows both intrinsic anchoring-induced easy axes. From the parabolic behavior close to both minima, the corresponding anchoring energy W_I can be estimated and expressed in terms of the de Gennes extrapolation length K/W_I. This length turns

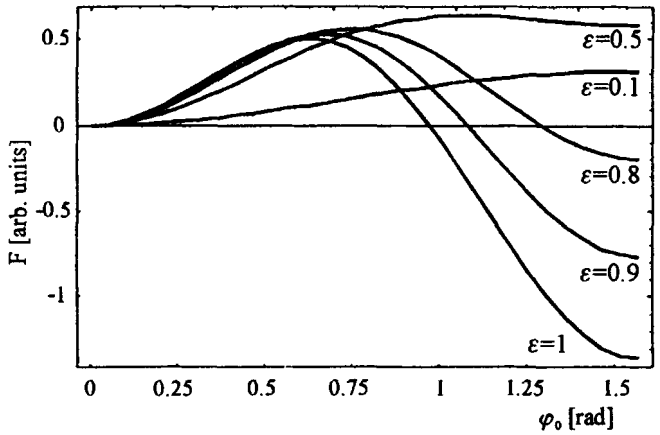

Figure 2: Energy of the undistorted sample vs. tilt angle φ_0 for different ε. All curves have been shifted to the same starting point at $\varphi_0 = 0$ rad. The sample thickness is equal to 100 layers. No external field applied.

out to be of the order of ~0.5 nm for $\varepsilon = 1$ and ~5 nm for $\varepsilon = 0.1$. On the other hand, experiments with real nematics yield $K/W_I > 100$ nm. In order to be sure that this gap is not a result of our simplified determination of the intrinsic anchoring strength we decided to simulate the effect of the external magnetic field. Close to the wall, the solution obtained by minimizing $F_i + F_m$ exhibits a deviation of the tilt angle from its field-determined bulk value. This effect is caused by the intrinsic anchoring. The deformation can be strong, if the applied magnetic field is strong enough. In the phenomenological picture we can replace this intrinsic anchoring with the usual Rapini-Papoular anchoring, which —

depending on the value of ε — favors either homeotropic or planar easy axis. Then all director profiles can be described by means of the standard Frank elastic theory, including this additional intrinsic anchoring term. The calculated director profiles are shown in Fig. 3 (dots). Solid lines denote the fit according to the Frank theory. From the parameters of the fit, it is again possible to extract the extrapolation length K/W_I, which is of the same order of magnitude for both values of ε as above. This thus leads to the conclusion that rather isotropic intermolecular interactions with $\varepsilon \ll 1$ are more appropriate for studying nematics. We expect that also the inclusion of thermal fluctuations would not change much this estimates.

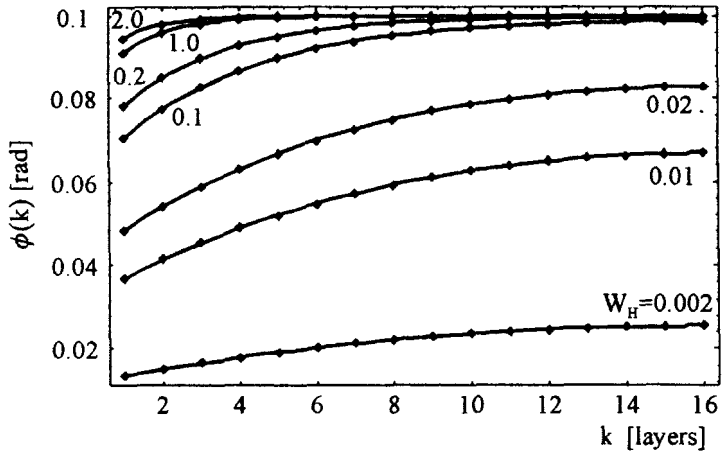

Figure 3: Director profiles for different values of $W_H \propto H^2$ (H is the strength of the magnetic field). The direction of the field is 0.1 rad. No external anchoring is applied, $\varepsilon = 0.1$. The sample thickness is equal to 31 layers.

In the next step we impose external anchoring $W_S \neq 0$ caused by the interaction between the nematic and the substrate. Now there is a competition of the intrinsic and external anchoring, which are both restricted to a thin subsurface layer. The result of this competition is a subsurface deformation whose characteristic length is only few molecular dimensions. For $\varepsilon \sim 1$, which — as shown above — implies far too strong intrinsic anchoring, the deformations can be strong. Therefore we limit further discussion to director profiles with $\varepsilon < 0.5$ (see Fig. 4). The deformations are weak although the competing anchorings are still rather strong. It is interesting to study how the amplitude of the subsurface deformation $\Delta\phi = \phi_b - \phi_s$ (where ϕ_b is the resulting bulk tilt angle) depends on the surface tilt angle ϕ_s. The dependences $\Delta\phi(\phi_s)$ for several ε are plotted in Fig. 5. Only for $\varepsilon \ll 1$ they exhibit a simple $\Delta\phi \propto \sin 2\phi_s$ dependence, which resembles the one predicted by elastic theory including a weak K_{13} term and a second order stabilizing term. We believe that instead of partially describing the behavior of $\Delta\phi$ in terms of K_{13} elasticity one can completely understand it (in the whole range of ε) in terms of competing

intrinsic anchoring and external anchoring or field alignment.

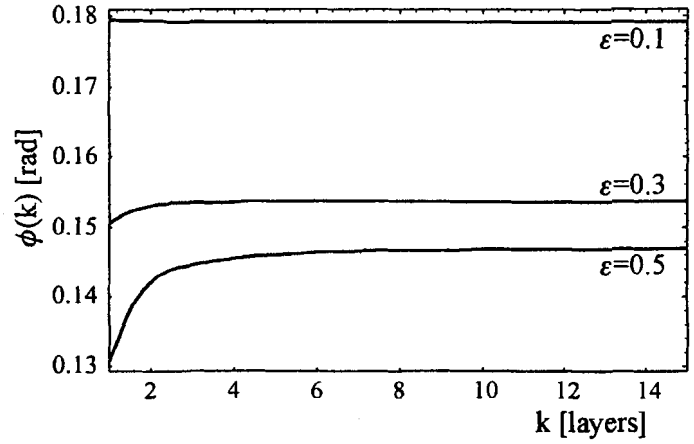

Figure 4: Director profiles for different ε. External anchoring of strength $W_S = 1$ and easy axis 0.2 rad are applied. No magnetic field is applied. The sample thickness is equal to 71 layers.

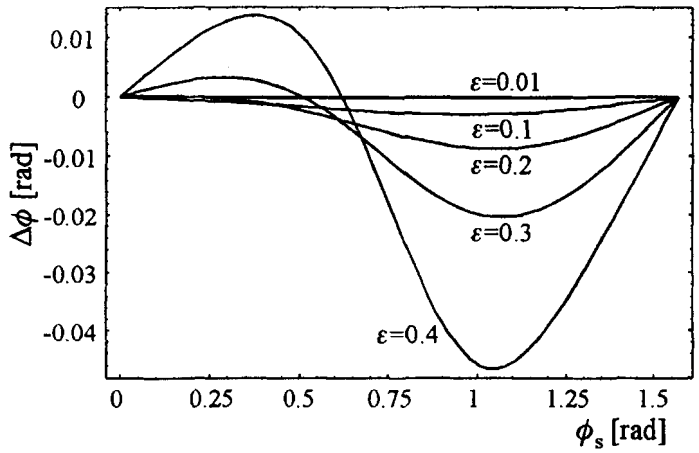

Figure 5: The amplitude of the subsurface deformation $\Delta\phi$ vs. the surface angle ϕ_s for different ε. External anchoring of strength $W_S = 1$ is applied. The sample thickness is equal to 31 layers.

Further, the results of our simulations prove a close connection between the strength of subsurface deformation and the strength of both intrinsic and external anchoring (or external field). The anchoring in real systems with extrapolation lengths > 100 nm indicates that the effective intermolecular interaction must have a small anisotropy ε and that subsurface deformations, if they exist, are weak.

3 Paranematic surface induced ordering

Surface induced ordering in the isotropic liquid crystal phase is particularly important in microconfined liquid crystals with high surface-to-volume ratio. The phenomenological theory of nematic ordering in confined geometries has been first used by Sheng [20, 21] and extended to more general form of nematic-substrate coupling by Sluckin and Poniewierski [22]. Similar approach has also been used in studies of nematic ordering in droplets [23] and wetting transitions in cylindrical cavities [24]. The phenomenological Landau-de Gennes theory is based on the assumption that in vicinity of the nematic-isotropic phase transition, the difference between the free energy densities of nematic and isotropic phase (f) can be expanded in terms of invariants of the order parameter $\mathsf{Q} = \mathsf{Q}(\mathbf{r}, t)$ (which is a symmetric, traceless second rank tensor)

$$f = \frac{1}{2}A(T - T^*)\,\mathrm{tr}\,\mathsf{Q}^2 - \frac{\sqrt{6}}{3}B\,\mathrm{tr}\,\mathsf{Q}^3 + \frac{1}{4}C\left(\mathrm{tr}\,\mathsf{Q}^2\right)^2 + \frac{1}{2}L\,\nabla\mathsf{Q}\vdots\nabla\mathsf{Q}, \tag{10}$$

where A, T^*, B, C and L are material constants and T is the temperature. In restricted geometries, the total free energy also depends on the interaction of the liquid crystal with the confining material, which is often modeled by

$$F_S = -\frac{1}{2}G\,\mathrm{tr}\,(\mathsf{Q} - \mathsf{Q}_s)^2, \tag{11}$$

where G is the strength of the interaction and Q_s is the preferred value of the order parameter at the substrate.

The tensor order parameter can be represented in a suitable base, which is spanned by 5 base tensors. For a homeotropic and uniaxial structure in planar geometry, an appropriate base is [25]

$$\mathsf{T}_0 = \frac{1}{\sqrt{6}}\begin{bmatrix} -1 & & \\ & -1 & \\ & & 2 \end{bmatrix}, \mathsf{T}_{-1} = \frac{1}{\sqrt{2}}\begin{bmatrix} 1 & & \\ & -1 & \\ & & \end{bmatrix}, \mathsf{T}_1 = \frac{1}{\sqrt{2}}\begin{bmatrix} & 1 & \\ 1 & & \\ & & \end{bmatrix},$$
$$\mathsf{T}_{-2} = \frac{1}{\sqrt{2}}\begin{bmatrix} & & 1 \\ & & \\ 1 & & \end{bmatrix}, \mathsf{T}_2 = \frac{1}{\sqrt{2}}\begin{bmatrix} & & \\ & & 1 \\ & 1 & \end{bmatrix}. \tag{12}$$

The projection of the tensor order parameter onto T_0 corresponds to the degree of order, its projections onto $\mathsf{T}_{\pm 1}$ are related to the biaxiality of the alignment, and the projections onto $\mathsf{T}_{\pm 2}$ describe the orientation of the director. In this case, the only nonvanishing coefficient in the expansion of the equilibrium structure $\mathsf{Q}(\mathbf{r}) = \sum_{i=-2}^{2} Q_i(\mathbf{r})\mathsf{T}_i$ is the scalar order parameter $Q_0(\mathbf{r})$ [21].

As an illustration of liquid crystalline structures between two flat substrates promoting homeotropic ordering, two typical equilibrium scalar order parameter profiles are shown in Fig. 6. Below the nematic-paranematic transition temperature T_{NP}, the equilibrium

structure is ordered. In the paranematic phase, which is stable at $T > T_{NP}$, the center of the layer is isotropic, but the value of the scalar order parameter at the substrate remains nematic-like. As the temperature is increased, the degree of order in the boundary layer decreases. If the layer is thick compared to the nematic correlation length, T_{NP} is practically equal to the bulk transition temperature T_{NI}.

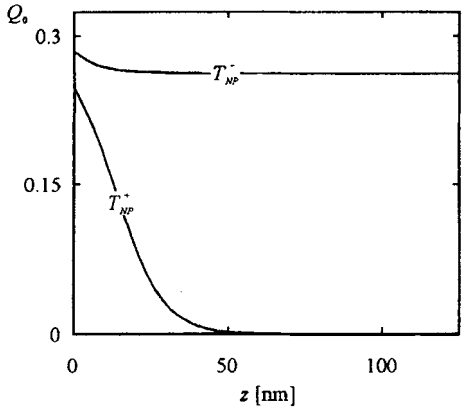

Figure 6: Scalar order parameter profiles of nematic and paranematic phase in planar homeotropic geometry for $A = 0.13 \times 10^6$ J/m^{3}K, $B = 1.59 \times 10^6$ J/m^3, $C = 3.92 \times 10^6$ J/m^3, $L = 9 \times 10^{-12}$ N, $d = 250$ nm, $\mathbf{Q}_s = 0.3\mathbf{e}_z \otimes \mathbf{e}_z$ and $G = 3.1 \times 10^{-4}$ J/m^2. In this case, $T_{NP} = T_{NI} + 1.0238(T_{NI} - T^*)$.

In the following, we present some recent experimental studies of the behavior of partially ordered microconfined liquid crystalline systems.

3.1 DNMR study of the orientational wetting transitions

This illustration of the importance of the phenomenological predictions is based on recent deuterium NMR study performed by Crawford et al. [26]. The cylindrical channels (0.2 μm in diameter) in 60 μm thick aluminum oxide (Anopore) membranes with chemically modified walls were permeated with the liquid crystal 4'-pentyl-4-cyanobiphenyl (5CB-αd_2) deuterated in the alpha position of the hydrocarbon chain. The cavity walls were chemically treated with aliphatic acids C_nH_{2n+1}-COOH with tail lengths from 5 to 20 carbons. Anopore membranes with 40% porosity are an ideal host material for studies of confined liquid crystals with integrative NMR technique.

The 2H-NMR spectra in the isotropic phase are a result of complete motional averaging over the cylinder because during NMR measurement, the molecules migrate over a distance large compared to the cylinder radius R. Since the cavity radius is large compared to the nematic correlation length, the curvature effects can be neglected. So the average splitting of the resonance lines is directly related to the adsorption parameter $\Gamma = \int Q_0(z)\mathrm{d}z$ and

is for the magnetic field along the pores given by

$$\langle \delta\nu \rangle = \kappa \frac{\Gamma}{R} \delta\nu_0, \tag{13}$$

where $\delta\nu_0$ is the splitting in the completely ordered nematic phase ($Q_0 = 1$) and the geometrical factor κ equals 1 for homeotropic and 2 for planar anchoring. Depending on the behavior of the adsorption parameter, wetting is usually characterized as partial if Γ remains finite on approaching the phase transition or complete if it diverges [23]. Experimental results, obtained by Crawford et al. [27] and presented in Fig. 7, indicate that surfactants with $n = 5$, 6, and 20 exhibit partial wetting whereas those with $n = 9 - 18$ give rise to quasicomplete wetting. The temperature dependence of $\langle \delta\nu \rangle$ can be understood on the basis of Landau-de Gennes theory. The equilibrium order parameter profiles for homeotropic director supplemented by a correction for the first molecular layer as described in a previous work [25] yield a very good fit of the data with only two free parameters, G and Q_s. The predicted temperature dependences of the surface value of the induced nematic order parameter $Q_0(0)$ are shown in the insets to Fig. 7. We see that the surfactants with $n = 5$ and 6 correspond to the degenerate planar anchoring with negative order parameter, which at $n \sim 7$ transforms to the homeotropic anchoring. The degree of surfactant-induced paranematic order increases with increasing n until at $n \sim 20$ this ability abruptly drops to zero.

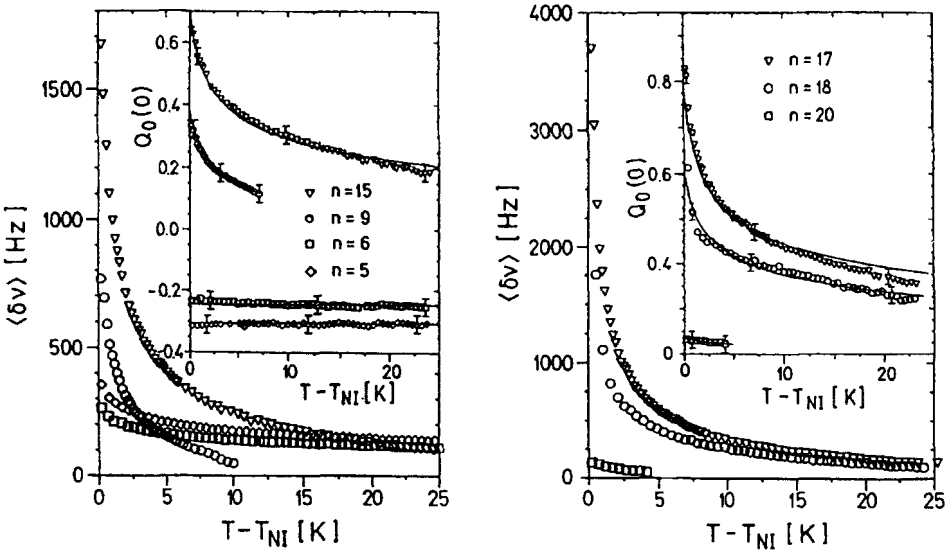

Figure 7: The temperature dependence of the splitting $\langle \delta\nu \rangle$ for various chain lengths of the surfactant C_nH_{2n+1}-COOH: $n = 5, 6, 9$, and 15 (left) and $n = 17, 18$, and 20 (right). In the insets, the temperature dependence of the value of the orientational order parameter at the surface is shown. Solid lines: theoretical fits (see text).

The behavior of the ordering power of the surface Q_s is shown in Fig. 8. The first

transition is a consequence of the change in the preferred anchoring direction. It is caused by the increasing thickness of the surfactant layer, which masks the aligning power of the substrate preferring planar anchoring and augments the strength of the homeotropic anchoring caused by surfactant itself. On the other hand, the second transition could be understood as an ordering transition in the surfactant layer when the chain length surpasses a critical value. The difference in the transition nature is also reflected in a drastic jump of the coupling constant G from 6×10^{-3} J/m^2 to 7×10^{-4} J/m^2 at $n \sim 7$ and no change at the other transition.

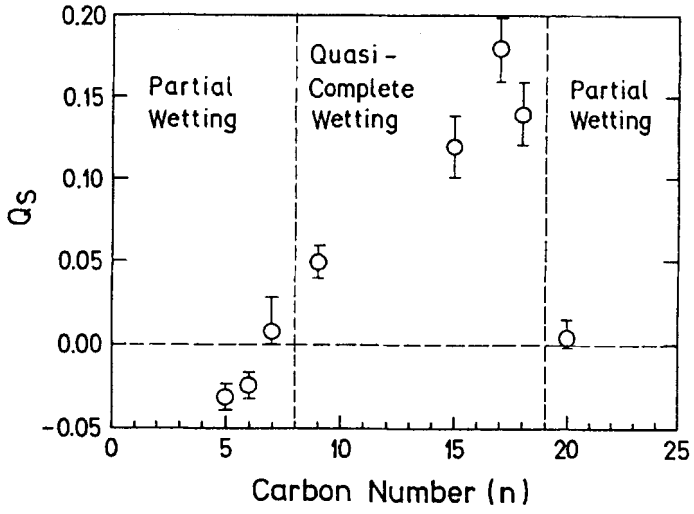

Figure 8: The preferred value of the order parameter at the surface (Q_s) as a function of surfactant chain length. The three regimes of wetting behavior are separated by dashed lines.

3.2 Fluctuations of tensor order parameter in paranematic layer

The low frequency DNMR relaxation study [28] has not been performed to such great detail as the line splitting investigation, but it indicates a precritical increase of the relaxation rate. The effect was explained by a relatively slow molecular exchange in the surface layer. However, slow order parameter fluctuations in a partially ordered boundary layer should be considered as well. Here we report on preliminary results of our study of fluctuations based on the Landau-de Gennes approach.

To simplify the analysis, a one dimensional system — a nematic liquid crystal between two infinite order inducing plates, parallel to the plane xy and located at $z = 0$ and $z = d$ — is considered. If the hydrodynamic degrees of freedom are neglected, the dynamics of

the nematic tensor order parameter is described by [28, 29]

$$\eta \frac{\partial \mathsf{Q}}{\partial t} = -A(T - T^*)\,\mathsf{Q} + \sqrt{6} B\,\mathsf{Q}^2 - C\mathsf{Q}\,\mathrm{tr}\,\mathsf{Q}^2 + L\nabla^2\mathsf{Q}, \tag{14}$$

where η is the viscosity coefficient, typically $\sim 10^{-2}$ Ns/m^2. In case of no dissipation of energy at both interfaces and for the surface free energy described by Eq. (11), the boundary conditions are given by $\pm L\mathsf{Q}' + G\,\mathsf{Q}_s - G\,\mathsf{Q} = 0$, where + and − correspond to $z = 0$ and $z = d$, respectively, and $'$ denotes $\mathrm{d}/\mathrm{d}z$.

The tensor order parameter is decomposed into its static and fluctuating part $\mathsf{Q}(\mathbf{r},t) \to \mathsf{Q}(\mathbf{r}) + \mathsf{A}(\mathbf{r},t)$, which can both be represented in above introduced base. Since the fluctuations of the ordering $\mathsf{A}(\mathbf{r},t) = \sum_{i=-2}^{2} a_i(\mathbf{r},t)\mathsf{T}_i$ are small, the equation of motion can be linearized. The eigenmodes of the fluctuations are sought in form $a_i(\mathbf{r},t) = \exp[i(k_x x + k_y y)]\alpha_i(z)\exp(-t/t_i)$, where t_i is the relaxation time of the mode. The perpendicular parts of the eigenmodes, $a_i(z)$'s, are determined by

$$\begin{aligned}
L\alpha_0'' - \left[A(T - T^*) - \frac{\tau_a}{\tau_0} - 2BQ_0 + 3CQ_0^2\right]\alpha_0 &= 0,\\
L\alpha_{\pm 1}'' - \left[A(T - T^*) - \frac{\tau_a}{\tau_{\pm 1}} + 2BQ_0 + CQ_0^2\right]\alpha_{\pm 1} &= 0,\\
L\alpha_{\pm 2}'' - \left[A(T - T^*) - \frac{\tau_a}{\tau_{\pm 2}} - BQ_0 + CQ_0^2\right]\alpha_{\pm 2} &= 0,
\end{aligned} \tag{15}$$

where $\tau_i^{-1} = t_i^{-1} - \frac{L}{\eta}\left(k_x^2 + k_y^2\right)$ are the reduced relaxation rates of the modes and $\tau_a = 2B^2\eta/9C$. The boundary conditions reduce to $\pm L\alpha_i' - G\alpha_i = 0$ with + applying at $z = 0$ and − at $z = d$.

In order to determine the spectrum of fluctuations of the ordering near the phase transition, Eqs. (15) are solved numerically and the result is depicted in Fig. 9 (the values of the material parameters are listed in caption to Fig. 6). For $T < T_{NP}$, the spectrum of normal modes is basically the same as in bulk nematic phase, corrected for the absence of the long wave length modes, which is due to confinement. Above the phase transition, the situation is quite different. The dispersion of the higher modes can be very well described by assuming that the system is perfectly isotropic (Fig. 9, $T > T_{NP}$). However, the elementary order parameter and director modes — just above the phase transition, these are both significantly slower than the others — cannot be accounted for by this simplified argument: they must be intimately related to the partially ordered boundary layer. As shown in Fig. 10, the two slow modes are localized at the boundary layer. The elementary order parameter mode obviously corresponds to fluctuations of the thickness of the boundary layer and the slowest director eigenmode represents fluctuations of alignment within the partially ordered boundary layer.

Thus, an order-inducing substrate can give rise to slow excitations in confined liquid crystals above the nematic-isotropic phase transition temperature. These modes correspond to fluctuations of thickness of the partially ordered boundary layer and to nematic director fluctuations within this region, respectively. Immediately above the transition temperature, the former can be significantly slower than the latter [30].

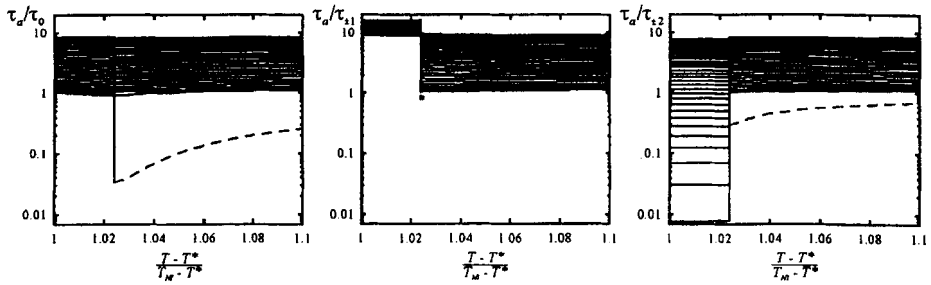

Figure 9: The spectrum of reduced relaxation rates of the tensorial fluctuations: order parameter (left), biaxiality (center), and director eigenmodes (right). (Only the lowest 30 modes of each kind are plotted.) The dynamics of the paranematic phase is characterized by two slow modes (left and right, dashed line).

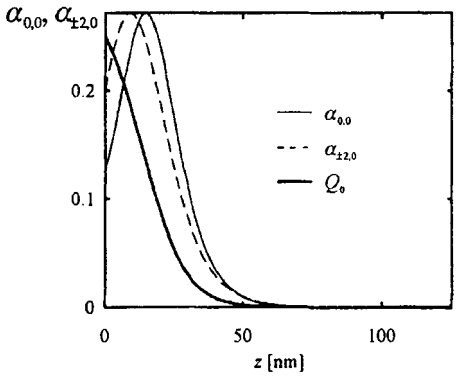

Figure 10: The two slow modes in paranematic phase at T_{NP}^{+}. The lowest order parameter eigenmode ($\alpha_{0,0}$) corresponds to fluctuations of thickness of partially ordered boundary layer and the elementary director mode ($\alpha_{\pm 2,0}$) represents fluctuations of alignment in the boundary layer. Thick line: the equilibrium scalar order parameter profile.

3.3 Forces in paranematic layers

In a recent experiment [31], the force between two solid objects immersed in the nematic liquid crystal has been measured using a modified atomic force microscope. Above the nematic-isotropic phase transition temperature, the magnitude of the observed attractive force is typically ~ 1 nN.

The liquid crystal can give rise to force, related to the substrate induced inhomogeneity of the ordering in the sample [22], and to Casimir attraction mediated by thermal fluctuations [32]. The former is expected to be short range and — as implied by preliminary calculations — the latter has longer range. At small distances between the two objects the nematic liquid crystal could exhibit superheated nematic and supercooled paranematic phases and, thus, a hysteresis in both inhomogeneity-induced and Casimir forces. In the following, some aspects of the inhomogeneity-induced force are presented.

The real experimental setup is modeled by a one dimensional geometry with nematic liquid crystal sandwiched between two parallel plates. The anchoring of the molecules at the boundaries is assumed to be homeotropic. The nematic director field is assumed to be uniform so that the liquid crystalline ordering can be described by the scalar order parameter Q_0. The equilibrium structures are determined by minimization of the above total free energy of the liquid crystal $F = \int f dV + F_S$. The stability of the nematic and paranematic phase depends on the distance between the plates.

The force between the two objects is given by the derivative of the total free energy of the LC with respect to the separation of the substrates (d) [22]. In Fig. 11, its dependence on d for 8CB is presented for various temperatures.

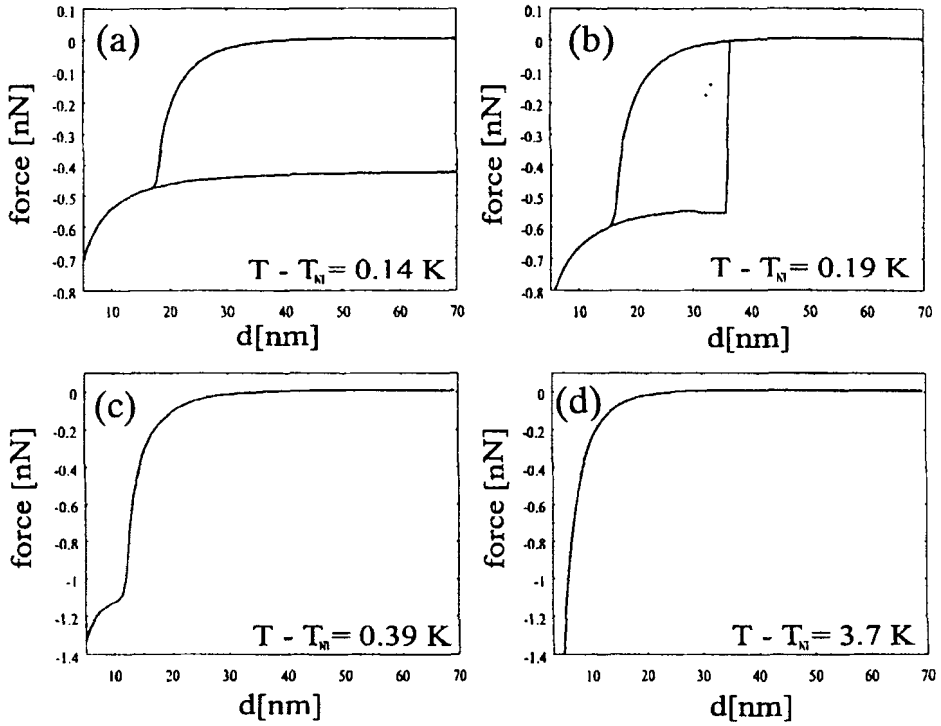

Figure 11: Force between two parallel substrates as a function of d for $Q_s = 0.5$ and $G = 2 \times 10^{-4}$ J/m^2. The effective area of the planes is equal to 0.36 μm^2.

In Fig. 11a, $T = T_{NI} + 0.14$ K. For small d, the liquid crystal can be found in nematic phase only and the force is therefore a single-valued function of d. For larger separation of the plates, both metastable nematic and stable paranematic phase may exist so that there are two regimes of the force. Since the maximum superheating temperature of the nematic phase in a bulk LC is $T_{NI} + 0.16$ K, the force in the metastable nematic phase tends to a constant but nonzero value at larger distances between plates (the hysteresis loop of the force is not closed). In Fig. 11b, $T = T_{NI} + 0.19$ K is above the maximum superheating temperature of the nematic phase in a bulk LC and the hysteresis loop is

closed. At higher temperatures (Fig. 11c; $T = T_{NI} + 0.39$ K), the hysteresis loop disappears. The discontinuity on the curve corresponds to the first order nematic-paranematic phase transition. For temperatures few K above T_{NI} (Fig. 11d), the knee disappears as well, since the only possible state of the liquid crystal for all d is the paranematic phase. In general, the force is attractive for small d's and (weakly) repelling for large d's.

The temperature dependence of the magnitude of the force for different values of Q_s and G is shown in Fig. 12 for 8CB. In case of weak substrate coupling (Fig. 12a; $G = 2 \times 10^{-5}$ J/m^2, $Q_s = 0.3$), the force decreases with temperature. For large Q_s (Fig. 12b; $G = 2 \times 10^{-5}$ J/m^2, $Q_s = 0.6$), the force exhibits a discontinuity, which corresponds to the nematic-paranematic transition. If the nematic-substrate coupling is strong (Fig. 12c; $G = 2 \times 10^{-4}$ J/m^2, $Q_s = 0.3$), the force between the substrates is a nonmonotonous function of temperature. Its maximum occurs approximately 0.5 K above T_{NI}.

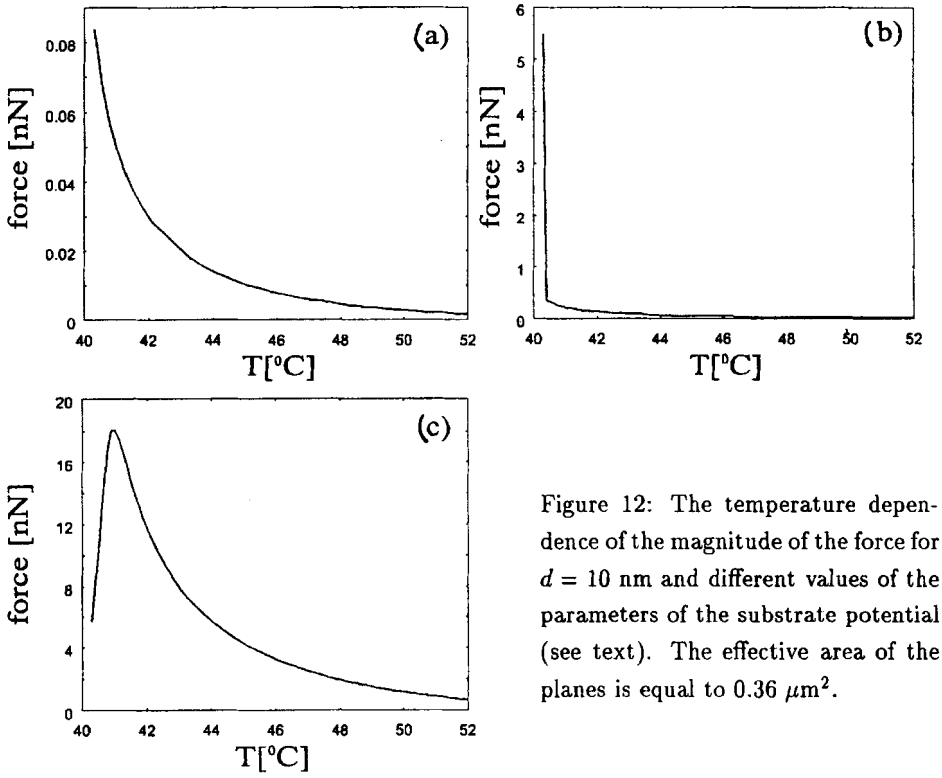

Figure 12: The temperature dependence of the magnitude of the force for $d = 10$ nm and different values of the parameters of the substrate potential (see text). The effective area of the planes is equal to 0.36 μm^2.

These theoretical predictions, based on a simplified model, explain a significant part of the experimentally observed force. However, for a complete understanding of the interaction of the two objects, mediated by the liquid crystal, Casimir force should be taken into account as well.

4 Conclusions

In the review, preliminary results of our recent studies of different aspects of surface affected ordering in microconfined liquid crystals are presented.

In order to broaden the current understanding of the splay-bend (K_{13}) elasticity in nematic liquid crystals and the corresponding predictions of strong subsurface deformations, the nematic ordering is studied on a molecular scale. The simulations imply that there is an intimate connection between the strength of the subsurface deformation and the strength of intrinsic anchoring, which results from incomplete molecular interaction at the wall. A comparison with anchoring strengths of real nematics indicates that the intermolecular interaction must have a small anisotropy. In such case, the resulting subsurface deformations are weak. As our predictions for subsurface deformations cannot be satisfactorily explained within the phenomenological K_{13} elasticity, we believe that a more microscopic description in terms of competing external and intrinsic anchoring is the most appropriate.

The usefulness of the Landau-de Gennes phenomenological theory is demonstrated in analyzing the DNMR data on surface-induced ordering in microconfined 5CB where two wetting transitions occur. The first one is related to the change in the preferred anchoring direction and the second transition is associated with the chain length induced ordering transition in the surfactant layer.

The phenomenological approach is also used to analyze the spectrum of the fluctuations in paranematic phase and the results indicate that an order-inducing substrate gives rise to slow excitations, which correspond to fluctuations of thickness of the partially ordered boundary layer. Within the same theoretical framework, the forces between solid objects, immersed in the nematic liquid crystal, are analyzed. It turns out that the force, mediated by the surface-induced order in a liquid crystal, can exhibit a variety of different behaviors.

Acknowledgments

The authors would like to thank G. Barbero and V. M. Pergamenshchik for stimulating discussions. Support from Ministry of Science and Technology of Slovenia (Grant No. J1-7067) and European Union (Grant-CT93-0159) is acknowledged.

References

[1] J. W. Doane, N. S. Vaz, B. G. Wu and S. Žumer, Appl. Phys. Lett. **48**, 269 (1986).

[2] J. L. Fergason, SID Digest **XVI**, 68 (1985).

[3] J. W. Doane, in *Liquid Crystals: Applications and Uses*, edited by B. Bahadur (World Scientific, Singapore, 1990).

[4] R. J. Ondris-Crawford, E. P. Boyko, B. G. Wagner, J. H. Erdmann, S. Žumer, and J. W. Doane, J. Appl. Phys. **69**, 6380 (1991).

[5] A. Golemme, S. Žumer, D. W. Allender, and J. W. Doane, Phys. Rev. Lett. **61**, 1937 (1988).

[6] G. P. Crawford, L. M. Steele, R. J. Ondris-Crawford, G. S. Iannacchione, C. J. Yaeger, J. W. Doane, and D. Finotello, J. Chem. Phys. **96**, 7788 (1992).

[7] G. S. Iannacchione, G. P. Crawford, S. Žumer, J. W. Doane, and D. Finotello, Phys. Rev. Lett. **71**, 2595 (1993).

[8] T. Bellini, N. A. Clark, C. D. Muzny, L. Wu, C. W. Garland, D. W. Schaefer, and B. J. Oliver, Phys. Rev. Lett. **69**, 788 (1992).

[9] S. Kralj, G. Lahajnar, A. Zidanšek, N. Vrbančič-Kopač, M. Vilfan, R. Blinc, and M. Kosec, Phys. Rev. E **48**, 340 (1993).

[10] E. Berggren, C. Zannoni, C. Chiccoli, P. Pasini, and F. Semeria, Chem. Phys. Lett. **197**, 224 (1992).

[11] E. Berggren, C. Zannoni, C. Chiccoli, P. Pasini, and F. Semeria, Phys. Rev. E **49**, 614 (1994).

[12] E. Dubois-Violette and E. Parodi, J. Phys. (Paris) **C4**, 57 (1969).

[13] D. W. Allender, G. P. Crawford, Phys. Rev. Lett. **67**, 1442 (1991).

[14] S. Kralj and S. Žumer, Phys. Rev. A **45**, 2461 (1992).

[15] C. Oldano and G. Barbero, J. Phys. Lett. **46**, 451 (1985).

[16] G. Barbero and A. Strigazzi, Liq. Cryst. **5**, 693 (1989).

[17] V. M. Pergamenshchik, Phys. Rev. E **48**, 1254 (1993).

[18] G. Barbero, L. R. Evangelista, and S. Ponti, Phys. Rev. E **53**, 1265 (1996).

[19] P. G. de Gennes and J. Prost, *The Physics of Liquid Crystals* (Clarendon Press, Oxford, 1993).

[20] P. Sheng, Phys. Rev. Lett. **37**, 1059 (1976).

[21] P. Sheng, Phys. Rev. A **26**, 1610 (1982).

[22] A. Poniewierski and T. J. Sluckin, Liq. Cryst. **2**, 281 (1987).

[23] S. Kralj, S. Žumer, and D. W. Allender, Phys. Rev. A **43**, 2943 (1991).

[24] G. P. Crawford, R. J. Ondris-Crawford, S. Žumer, J. W. Doane, Phys. Rev. Lett. **70**, 1838 (1993).

[25] V. L. Pokrovski and E. I. Kac, Zh. Eksp. Teor. Fiz. **73**, 774 (1977).

[26] G. P. Crawford, R. J. Ondris-Crawford, J. W. Doane, and S. Žumer, Phys. Rev. E **53**, 3647 (1996).

[27] N. Vrbančič, M. Vilfan, R. Blinc, J. Dolinšek, G. P. Crawford, and J. W. Doane, J. Chem. Phys. **98**, 3540 (1993).

[28] L. D. Landau and I. M. Khalatnikov, Dokl. Akad. Nauk SSSR **96**, 469 (1954).

[29] S. Hess, Z. Naturforsch. **30 a**, 728 (1975).

[30] P. Ziherl and S. Žumer, Phys. Rev. Lett. **78**, 682 (1997).

[31] I. Muševič, G. Slak, and R. Blinc, presented at 16th International Liquid Crystal Conference, Kent, 1996.

[32] A. Ajdari, B. Duplantier, D. Hone, L. Peliti, and J. Prost, J. Phys. II France **2**, 487 (1992).